Distal Pocket Polarity in Ligand Binding to Myoglobin: Deoxy and Carbonmonoxy Forms of a Threonine^{68}(E11) Mutant Investigated by X-ray Crystallography and Infrared Spectroscopy†,‡

Alexander D. Cameron, Stephen J. Smerdon,§ and Anthony J. Wilkinson*

Department of Chemistry, University of York, Heslington, York YO1 5DD, U.K.

Jarjis Habash and John R. Helliwell

Department of Chemistry, University of Manchester, Manchester M13 9PL, U.K.

Tiansheng Li and John S. Olson

Department of Biochemistry and Cell Biology and the W. M. Keck Center for Computational Biology, Rice University, Houston, Texas 77251-1892

Received July 7, 1993; Revised Manuscript Received September 21, 1993®

ABSTRACT: The crystal structures of the deoxy and carbonmonoxy forms of a distal pocket myoglobin mutant in which valine^{68}(E11) is replaced by threonine have been solved to 2.1- and 2.2-Å resolution, respectively. This substitution has been shown previously to cause large decreases in the rate of oxygen binding and to lower the equilibrium association constants for O_2 and CO. The synchrotron Laue method was used for the rapid acquisition of X-ray diffraction data to overcome problems caused by the very rapid rate of autooxidation of the mutant protein. The refined deoxy structure shows that the noncoordinated water molecule in the distal pocket is in a position to form strong hydrogen bonds with both the N_ϵ-H of the distal histidine^{64} and O_γ of threonine^{68} with no other unexpected alterations in the protein structure. In the carbonmonoxy form, the bound ligand is well-defined and inclined away from the two hydrogen-bonding groups, refining to a position in which the Fe–C–O angle is 162°. This value is very close to that previously observed in recombinant wild-type and position-64 (E7) mutants of sperm whale myoglobin (160–170°). The similarity of the CO conformations contrasts with the 150-fold range in equilibrium binding constants (K_{CO}) among the distal pocket myoglobin mutants and indicates that CO affinities cannot be predicted from the coordination geometry of the bound ligand. Furthermore, a comparison of the infrared stretching frequencies of CO in wild-type, valine^{64} and threonine^{68} single mutant, and valine^{64}–threonine^{68} double mutant pig carbonmonoxymyoglobins shows a lack of correlation between K_{CO} and ν_{CO}. These effects can be understood in terms of the stability of noncovalently bound water in deoxymyoglobin and electrostatic interactions between bound ligands and the distal pocket residues.

Early comparisons of the crystal structure and solution properties of myoglobin with those of chelated model heme compounds suggested that steric hindrance by the polypeptide portion of the protein plays a dominant role in determining the rate and equilibrium ligand-binding parameters. Firstly, the iron atom in the crystal structure of myoglobin is recessed in the protein and inaccessible to the bulk solvent so that conformational fluctuations in the protein are required for ligand entry (Takano, 1977; Phillips, 1980, 1981; Kuriyan et al., 1986). The rate of O_2 binding to myoglobin is 10–20-fold slower than its rate of binding to chelated model heme compounds, implying that the structural barrier is also a kinetic barrier (Mims et al., 1983). Secondly, the distal histidine^{64}-(E7) side chain has been proposed to play a key role in lowering the affinity of myoglobin for CO by hindering this ligand sterically from adopting the linear Fe–C–O conformation observed in model heme compounds (Kuriyan et al., 1986; Peng & Ibers, 1976). These interpretations are, however, complicated by the presence of a well-ordered water molecule which resides in the distal heme pocket of deoxymyoglobin in hydrogen-bonding distance of N_ϵ-H of histidine^{64}. As a result, the overall ligand-binding process should be viewed as a displacement reaction in which noncoordinated water is replaced by the coordinated ligand.

Recent studies have employed directed mutagenesis methods to evaluate the contributions of individual side chains to the ligand-binding kinetics and equilibria (Springer et al., 1989; Egeberg et al., 1990; Carver et al., 1991, 1992; Smerdon et al., 1991). The emerging conclusion from these studies is that polarity in the distal heme pocket rather than steric hindrance is the major determinant of the O_2 association rates. Replacement of the distal histidine^{64}(E7)[1] in sperm whale myoglobin by a series of apolar residues leads to large increases in the overall ligand-binding rates, which approach those of chelated model heme compounds (Springer et al., 1989). Only modest changes in the kinetics were observed for a mutant

† This research was supported by Grant GR/E 98867 from the SERC, U.K. (A.J.W.), by SERC studentship 89305229 (A.D.C.), by grants from the SERC Molecular Recognition Initiative and the Hasselblad Foundation (J.R.H.), and by United States Public Health Grant GM-35649, HL-47020, Grant C-612 from the Robert A. Welch Foundation, and the W. M. Keck Foundation.

‡ The coordinates and structure factors for the deoxy and carbonmoxy forms of the threonine^{68} pig myoglobin mutants have been deposited in the Brookhaven Protein Data Bank. The identification codes are 1YCA and 1YCB, respectively.

§ Present address: Department of Molecular Biophysics and Biochemistry, Yale University, New Haven, CT 06511.

® Abstract published in *Advance ACS Abstracts*, November 15, 1993.

[1] Nomenclature of Dickerson and Geis (1983).

0006-2960/93/0432-13061$04.00/0

with glutamine occupying position-64. In contrast, increasing distal pocket polarity by replacing valine^{68}(E11) with threonine in pig myoglobin leads to a reduction in the overall rate of oxygen binding. These effects have been interpreted in terms of the changes in stability of the noncovalently bound water molecule in the distal pocket of deoxymyoglobin. Stabilization of this water through hydrogen bonding either to histidine^{64} or to threonine^{68} in the case of the mutant protein is expected to inhibit its displacement by ligands and to destabilize the ligated states with respect to deoxymyoglobin.

The isosteric, valine^{68}-to-threonine mutation serves as a particularly useful probe of the role of distal pocket polarity (Smerdon et al., 1991). This substitution causes 3–4-fold increases in the oxygen and carbon monoxide dissociation rate constants and lowers the affinity of the mutant protein for these ligands 17-fold and 5-fold, respectively. A marked decrease in the association rate constant for O_2 binding was also observed. Tentative interpretations of these changes have been made on the basis of the pattern of hydrogen bonding observed in the crystal structure of the threonine^{68} mutant in the aquomet ferric form (Smerdon et al., 1991).

More rigorous interpretation of these observations requires a knowledge of the structure of the mutant protein in its ferrous forms. Here we report the determination of the crystal structures of the deoxy and carbonmonoxy forms of the threonine^{68} pig myoglobin mutant using the synchrotron Laue method to overcome problems associated with the rapid rate of autooxidation of these crystals. We have also recorded infrared stretching frequencies for bound CO in wild-type, threonine^{68}, valine^{64}, and valine^{64}–threonine^{68} pig carbonmonoxymyoglobins and compared these data with the crystal structures of threonine^{68} and several position-64 carbonmonoxymyoglobin mutants. The results show a surprising lack of correlation between the C–O stretching frequencies, Fe–C–O geometry in the crystal, and CO affinity. The data presented suggest that polarity rather than steric hindrance is the dominant factor in determining ligand affinities in myoglobin.

MATERIALS AND METHODS

Protein Purification, Characterization, and Crystallization. Recombinant wild-type and mutant pig myoglobins were purified in their aquomet forms as described previously (Smerdon et al., 1991). Association and dissociation rate constants for the binding of O_2 and CO to the valine^{64} and valine^{64}–threonine^{68} mutant proteins were measured according to the methods described by Rohlfs et al. (1990).

Crystals of the threonine^{68} mutant myoglobin were grown in hanging drops by vapor diffusion from 100 mM sodium phosphate buffer, pH 7.1, 70–80% ammonium sulfate and 5–6 mg/mL protein in the presence of a 50-fold molar excess of sodium dithionite under 1 atm of argon in a glovebox. These deoxymyoglobin crystals, typically of dimensions 0.6 × 0.4 × 0.15 mm^3, were mounted under argon in glass capillaries with a small column of ammonium sulfate/sodium dithionite on either side of the crystals. To maintain rapidly autooxidizing position-64 mutants of sperm whale myoglobin in the deoxy form, Quillin et al. (1993) used a flow cell to pass dithionite containing buffer over the crystals during data collection. Data collection from crystals of the threonine^{68} deoxymyoglobin mutant presents similar problems; autooxidation of threonine^{68} myoglobin is 50-fold faster than that of the wild-type pig protein, and the process is accelerated by exposure to X-rays (Brantley et al., 1993). These problems could not be overcome using a variety of crystallization and crystal handling regimes, and, instead of using a flow-cell setup, we have used synchrotron Laue methods to acquire data sets rapidly. Small changes in protein and solvent structure have been reliably deduced from electron density maps calculated using Laue data (Hadju et al., 1987; Schlichting et al., 1990; Scheidig et al., 1991; Lindahl et al., 1992; Singer et al., 1993). MbCO[2] crystals were grown in a similar manner to the deoxyMb crystals with the exception that the buffers were preequilibrated with CO. These crystals are somewhat more stable following exposure to X-rays.

Table I: X-ray Data Collection and Processing Statistics

	threonine^{68} MbCO	threonine^{68} deoxyMb
wavelength range used in LAUENORM (Å)	0.54–0.92	0.55–0.92
crystal-to-film distance (mm)	150	150
exposure time (s)	10	15
number of film packs	24	19
number of crystals	2	2
cell dimensions (space group $I2_1$[a])	a = 124.2 Å b = 42.5 Å c = 92.1 Å β = 92.2°	a = 124.6 Å b = 42.5 Å c = 92.0 Å β = 92.0°
d_{min} (Å)	2.2	2.1
number of reflections used in AGROVATA	46 118	36 760
number of independent reflections	17 828	18 251
mean $I/\sigma(I)$	5.89	5.17
percentage of reflections with $I > 3\sigma(I)$	85.3	77.8
percentage of theoretical reflections observed (∞ to d_{min})	72	63
percentage of theoretical reflections ($d_{min} < d < 2d_{min}$)	77	67
percentage of theoretical reflections ($d > 2d_{min}$)	39	38
R_{merge} (%)	8.7	11.1

[a] For convenience, we chose to process the data in the nonstandard space group $I2_1$, in which the β angle is close to 90°, rather than to process the data in the $C2$ cell, in which β = 128° and the a dimension is 157 Å.

Data Collection. The details of the data collection and processing are presented in Table I. For both the CO and the deoxymyoglobin crystals, data were collected at –4 °C on beamline 9.5 at the SRS Daresbury Laboratory (Brammer et al., 1988). A data set previously collected on a crystal of the aquomet form of the threonine^{68} mutant protein demonstrated the efficacy of using Laue radiation to observe small changes in the protein structure. These experiments showed that while the full spectral range of the beam ($\lambda \approx 0.5$–2.6 Å) allowed a data set to be collected very rapidly (total exposure time of 1.5 s), the poorer peak-to-background ratios meant that the weaker reflections could not be measured and that the data could only be processed to d_{min} = 2.7 Å. For data collection from the ferrous crystals, therefore, a 1-mm thickness of aluminum was placed in the synchrotron white beam to attenuate the higher wavelength X-rays and prolong crystal lifetime. Individual exposure times were increased from 0.15 to 10–15 s. Data were recorded at 6-deg intervals on packs of four films with a 0.2-mm section of aluminum placed between the third and fourth films of each pack to reduce the number of intensity overloads (Table I). The threonine^{68} MbCO data were collected from two crystals mounted so that the b^* and c^* axes were parallel to the spindle axis, respectively. The threonine^{68} deoxyMb crystals were more radiation sensitive, though data could still be collected from two crystals. These were mounted with the b^* axis parallel to the spindle axis. All of the crystals were periodically translated to reduce

[2] Abbreviations: rms, root mean square; MbCO, carbonmonoxymyoglobin; deoxyMb, deoxymyoglobin; MbO_2, oxymyoglobin.

the effects of radiation damage. The time elapsed between the first and last exposure of any section of crystal to the X-ray beam was generally 2 min but was occasionally 30 min. There was no obvious color change in any of the crystals, suggesting that if any autooxidation had taken place in the course of data collection, it was not extensive.

Data Processing. Films were digitized on a Joyce-Loebl Scandig-3 microdensitometer using a 50-μm raster. Data were processed in the nonstandard space group $I2_1$ using the Laue processing suite of programs developed at the Daresbury laboratory (Helliwell et al., 1989). Crystal orientations were determined from the positions of seven nodal spots widely distributed on each film using the programs SPOTIN and NEWLAUE. The unit cell and missetting angles were refined in the program GENLAUE, which then predicted the positions of the diffraction maxima. The spots (singles only) were integrated and profile-fitted in the program INTLAUE on a pack-by-pack basis, and the films within each peak were scaled in the program AFSCALE in three wavelength ranges and corrected for Lorentz, polarization, and obliquity effects. Finally, the packs were scaled together in the program LAUENORM, where the intensities of the reflections were also normalized with respect to the wavelength at which they were produced. Symmetry-related reflections were averaged, and structure factors were output using the programs ROTAVATA and AGROVATA (CCP4, 1986). Problems were encountered when the b^* axis of the crystal was parallel to the X-ray beam, owing to the lack of high-angle nodal reflections, which prevented two packs recorded from the MbCO crystals from being processed. The details of the processing and the completeness of the data are given in Table I.

Refinement of the Threonine^{68} MbCO Structure. The starting model for the refinement of the threonine^{68} MbCO structure was the wild-type metmyoglobin model refined against 1.75-Å data (Oldfield et al., 1992; Brookhaven PDB entry 1MYG). All solvent molecules were deleted from the model, as were the coordinated water molecules in the two protein molecules of the asymmetric unit. The occupancies of the atoms of valine^{68} were set to 0 along with side-chain atoms of residues with more than one conformation. The initial R_{cryst}[3] was 28.7% for all data between 10- and 2.2-Å resolution. Details of the course of refinement are set out in Table IIA. Five cycles of atomic positional refinement were carried out, with high weighting of the geometric terms to the X-ray terms in the program PROLSQ (Hendrickson & Konnert, 1980). Examination of $2F_o - F_c$ maps displayed on an Evans and Sutherland ESV10 using the program FRODO (Jones, 1982) showed breaks in both main- and side-chain electron density, and in various places the position of the density was inconsistent with the model. Prior to any rebuilding, the effects of the missing low-resolution data (Table I) were assessed by calculating maps from the wild-type metmyoglobin structure factors and coordinates, using only the 16 301 observations with *hkl* indices represented in the threonine^{68} MbCO data set. Since these maps showed similar discrepancies between the electron density and the model, it was concluded that the breaks in the electron density maps result from missing X-ray data rather than poor quality data. As these discrepancies were not generally apparent in $F_o - F_c$ maps, rebuilds were carried out into "omit" maps calculated with 20 or so residues removed at a time from the phasing.

[3] $R_{cryst} = \sum_{hkl}||F_{obs}| - |F_{calc}||/\sum_{hkl}|F_{obs}|$, where $|F_{obs}|$ and $|F_{calc}|$ are the observed and calculated structure factors of a reflection *hkl*, respectively. $R_{merge} = \sum|I_i - I_n|/\sum I_n$ where I_i is an intensity *hkl* and I_n is the average of the observed equivalents.

Table II: Progress of Refinement of the Threonine^{68} MbCO and the Threonine^{68} deoxyMb Structures[a]

A. Refinement of the Threonine^{68} MbCO Structure

no. and type of cycles	resolution range (Å)	no. of atoms (including water molecules)	no. of water molecules	average B value (Å^2)	R_{cryst} (%)
5 *x,y,z*	10–2.2	2440	0	23.0	24.2
Rebuild 1: CO and Threonine^{68} Built into the Electron Density					
5 *x,y,z*	10–2.2	2380	67	21.2	21.3
2 *x,y,z,B*[b]	6–2.2			19.7	21.1
Rebuild 2					
3 *x,y,z*	10–2.2	2497	97	16.9	20.9
2 *x,y,z,B*				18.9	20.0
Rebuild 3					
6 *x,y,z*	10–2.2	2523	103	17.3	19.7
Rebuild 4					
3 *x,y,z*	8–2.2	2502	107	16.9	19.5
2 *x,y,z,B*				19.2	18.8

B. Refinement of the Threonine^{68} deoxyMb Structure

no. of cycles	resolution range (Å)	no. of atoms	no. of water molecules	average B value (Å^2)	R_{cryst} (%)
5 *x,y,z*	6–2.3	2291	0	17.5	25.4
Rebuild 1: Threonine^{68} and Heme Fitted into the Electron Density					
5 *x,y,z*	6–2.3	2335	47	19.1	21.1
Rebuild 2					
5 *x,y,z*	6–2.3	2437	74	18.6	19.7
Rebuild 3					
5 *x,y,z*	8–2.1	2463	92	17.7	21.4
Rebuild 4					
3 *x,y,z*	8–2.1	2476	106	17.7	21.3
2 *x,y,z,B*[b]	6–2.1			18.8	20.8
Rebuild 5					
3 *x,y,z*	7–2.1	2482	109	17.4	20.1
2 *x,y,z,B*				19.3	19.7

[a] For the deoxymyoglobin refinement, the data were originally processed to d_{min} = 2.3 Å. This data set had an R_{merge}[3] of 10.3%, contained 14 832 independent reflections, and was 68% complete. Following rebuild 3, the data were reprocessed to d_{min} = 2.1 Å (see Table I), with the omission of the film batch most affected by radiation damage. The wavelength cutoff was also increased from 0.54 to 0.55 Å. [b] Prior to the refinement of the isotropic temperature (B) factors of individual atoms, the B-factors were averaged and truncated as described in the text.

In the first rebuilding session, threonine^{68} was modeled together with the CO ligand. In this and subsequent rebuilds, the atoms of any side chains for which electron density was not apparent were set to zero occupancy, while water molecules and side-chain atoms were introduced where positive F_o-F_c electron density was present. As few changes as possible were introduced into the model, in view of the close agreement between the structure factors for the mutant crystal and those of the wild-type crystal and the accurate refinement of the latter structure. The Fe–C and C–O bond lengths were restrained to 1.8 and 1.2 Å, respectively, and restraints were applied to maintain the Fe–C–O bond angle close to 180°, as observed in model heme compounds. After the initial stages of refinement, the individual atomic temperature factors were averaged over the main-chain and side-chain atoms on a residue by residue basis. Average B values outside the ranges of $0 < B < 20$ Å^2 for main-chain atoms and $10 < B < 40$ Å^2 for side-chain atoms were reset to lie within these limits. Cycles of restrained isotropic B-factor refinement were subsequently introduced into the least-squares minimization protocol (Table IIA).

Refinement of the Threonine^{68} deoxyMb Structure. The starting model for refinement against the deoxymyoglobin data was the refined structure of the threonine^{68} MbCO. The

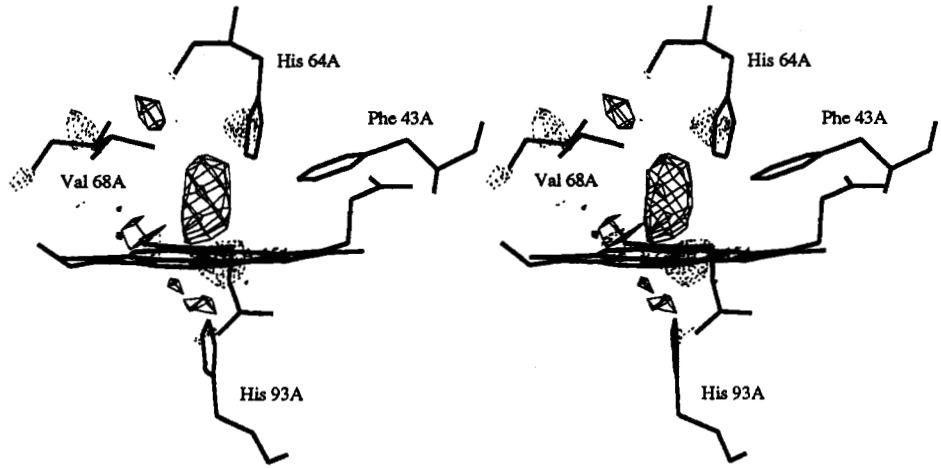

FIGURE 1: Stereo view of the initial threonine[68]-MbCO electron density map calculated with coefficients $F_{obsCOThr68} - F_{calcwt}$ and α_{calcwt} contoured at 3σ (thin lines) and -3σ (dotted lines). The map is displayed in the vicinity of the heme pocket of the A molecule and is superimposed on the wild-type aquometmyoglobin model (thick lines). In this and subsequent figures, the view is from the back of the heme pocket, showing the heme itself, histidine[64], valine[68], and phenylalanine[43] in the distal pocket and the coordinating histidine[93] on the proximal side. The electron density associated with the CO ligand is prominent, and there is both positive and negative density adjacent to the substituted valine side chain.

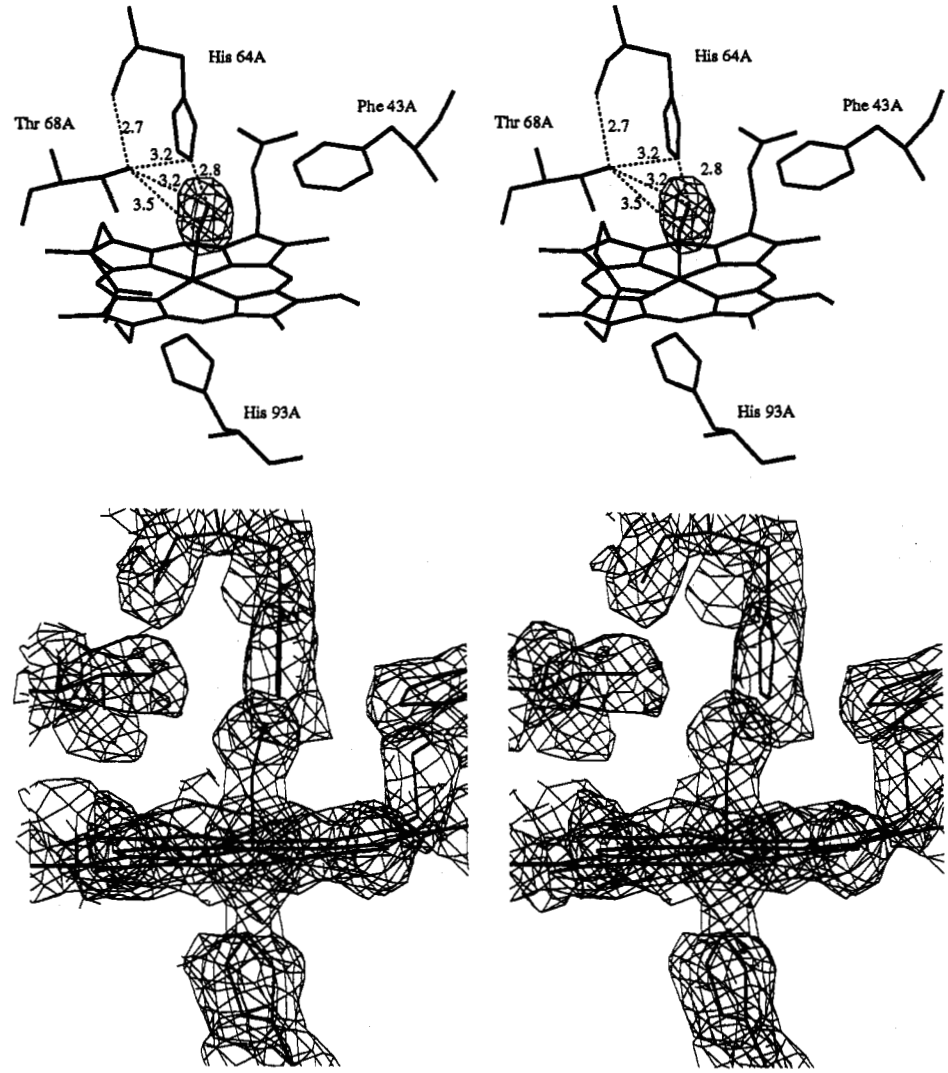

FIGURE 2: Stereo diagrams showing the structure and associated electron density (thin lines) in the heme environment of the A molecule of the refined threonine[68] MbCO structure: (top) $F_o - F_c$ density, contoured at $+3\sigma$, calculated following the removal of the CO atoms from the final refined coordinate set. The heights of the electron density peaks associated with the ligands, in the A and B molecules respectively are 2.4 and 3.0 times the highest noise peak in the map. The indicated interatomic distances are in angstroms. (bottom) $2F_o - F_c$ density calculated with all atoms included in the phasing and contoured at the 1σ level. The maps are closely similar in the heme environment of the B molecule (data not shown).

CO and solvent molecules were deleted from the structure, and the occupancies of the heme atoms and the atoms of the threonine[68] side chains were set to 0 in both molecules of the asymmetric unit. Following five cycles of positional refinement, the initial R_{cryst} of 29.5% fell to 25.4% for all data between 6- and 2.3-Å resolution (Table IIB). The heme group

and the threonine side chain were built into F_o-F_c maps; however, at this stage the electron density did not define the distal pocket water structure unambiguously, particularly in the A molecule where we noted, as before, that the $2F_o$-F_c maps were affected by the missing X-ray terms. Therefore, subsequent steps in the refinement were carried out with these water molecules omitted from the model so as to avoid biasing the structure. Distal pocket water molecules were not introduced until the final rebuild, when the program PEAKMAX (CCP4, 1986) was exploited to determine the centers of the peaks.

FTIR Spectroscopy. CO myoglobin samples were prepared as follows. A small amount of solid sodium dithionite was added to solutions of either ferric or ferrous myoglobins to remove oxygen and reduce the protein. The resultant deoxymyoglobin solution was then passed down a Sephadex G25 column equilibrated with 0.1 M phosphate, pH 7.0, 1 mM EDTA buffer that was saturated with 1 atm of CO gas to remove excess dithionite and its reaction products. The MbCO was concentrated to 3–5 mM in heme. Before FTIR spectra were collected a few grains of solid dithionite were added to ~60 μL of the MbCO solution, and the sample was reequilibrated with 1 atm CO for 2–3 min. The solution was slowly added to the FTIR windows (Wilmad 116-2 with a 56-μm spacer) which had previously been purged with nitrogen gas to remove air. Care was taken to ensure a uniform film thickness. IR spectra at 2-cm^{-1} resolution were collected in the region 1800–2100 cm^{-1} on a Mattson Galaxy 6020 spectrometer interfaced with a Compaq 386 computer. Up to 10 000 interferrams were collected for all samples and the corresponding buffers. The FTIR spectra of MbCO complexes were corrected for the buffer background by using the method of digital difference spectroscopy and then were adjusted for flat base lines.

RESULTS

Threonine^{68} MbCO Structure. The structure factor amplitudes for the threonine^{68} MbCO crystals agree more closely with data collected from wild-type metmyoglobin crystals than they do with data from threonine^{68} metmyoglobin crystals; the mean isomorphous differences are 18.9% and 34.2%, respectively. Experience with recombinant pig myoglobin crystals has shown a frequent lack of isomorphism between crystals from different batches that arises from relative rotations of the molecules of the asymmetric unit with respect to one another. Figure 1 shows the initial electron density map in the region of the distal pocket of the A molecule, calculated with coefficients $F_{obsCOThr68} - F_{calcwt}$ and α_{calcwt} with all water molecules removed from the wild-type structure. Peaks consistent with both bound CO and with a rotation of threonine^{68} in the mutant relative to valine^{68} in the wild-type protein are evident.

The final threonine^{68} MbCO structure comprising 2502 atoms, including 107 waters, has an R_{cryst} of 18.9% for 17 767 reflections between 8- and 2.2-Å resolution and satisfactory stereochemistry, as shown in Table III. Luzzati (1952) plots of the R_{cryst} as a function of resolution provide an upper estimate of the mean coordinate error of 0.2–0.25 Å. This value can be compared with the rms deviation of 0.18 Å in the positions of the C_α atoms of residues 3–145 in the A and B molecules after the chains have been superimposed. Figure 2 shows the electron density for the heme and the ligand in the A molecule of the asymmetric unit of the refined structure. Relative to the γ2 methyl group of valine^{68} in the wild type protein, the hydroxyl group of threonine^{68} in the mutant MbCO is 0.5 Å closer to the >C=O of histidine^{64}, due to a relative rotation about the C_α–C_β bond of the position-68 side chain. This arrangement is also noticeable in the crystal structure of the aquomet form of threonine^{68} myoglobin (Smerdon et al., 1991). The hydroxyl group of the threonine appears to donate a hydrogen bond to the main-chain carbonyl oxygen of histidine^{64}. As a result, the nonbonded electron pairs on the oxygen of the hydroxyl are oriented toward the nearby carbon and oxygen atoms of the ligand. Kinetic measurements suggest

Table III: Root Mean Square Deviations of the Final Model Parameters Relative to the Restraints Applied during Refinement

	threonine^{68} MbCO		threonine^{68} deoxyMb		
	rms deviation	no. of parameters	rms deviation	no. of parameters	target value
Distance Restraints (Å)					
bonds (1–2)	0.020	2456	0.020	2435	0.020
angles (1–3)	0.054	3331	0.055	3302	0.040
planar (1–4)	0.079	902	0.081	882	0.060
metal coordination	0.009	2	0.073	2	0.100
planar groups (Å)	0.015	422	0.016	418	0.020
chiral centers (Å)	0.144	348	0.138	348	0.120
Nonbonded Contacts (Å)					
single torsion	0.215	955	0.227	962	0.500
multiple torsion	0.224	743	0.239	738	0.500
possible hydrogen bond	0.227	201	0.249	217	0.500
Torsion Angles (deg)					
planar (0,80°)	2.643	306	2.843	304	20.000
staggered (±60,120°)	21.617	412	20.949	403	20.000
orthonormal (±90°)	40.557	38	40.064	1376	20.000
Thermal Restraints (Å^2)					
main-chain bond (1–2)	0.909	1388	0.856	1376	1.000
main-chain angle (1–3)	1.496	1738	1.387	1720	1.500
side-chain bond	1.953	1070	1.673	1061	1.500
side-chain angle	3.032	1591	2.503	1591	2.000

Table IV: Comparison of Interatomic Distances and Angles in the Heme Pocket of the Two Molecules of the Pig Threonine^{68} MbCO Asymmetric Unit with Those in Native and Wild-Type Sperm Whale Carbonmonoxymyoglobin

	pig threonine^{68} MbCO		sperm whale MbCO	
	A molecule	B molecule	native[a]	wild-type[b]
Angles (deg)				
Fe–C–O (θ)[c]	162	163	140, 120	169
NC_{porph}–Fe–C	91	90	90	93
NC–Fe–C–O (φ)[d]	9	32	−62, 60	44
Distances (Å)				
Fe–histidine^{93} N_ϵ	2.1	2.1	2.2	2.3
Fe–C	1.8	1.8	1.9	1.9
Fe–plane of pyrrole nitrogens[e]	−0.10	0.01	0.00	0.05
histidine^{64} N_ϵ–O	2.8	2.9	2.7, 3.9	3.1
histidine^{64} N_ϵ–C	3.0	3.2	3.2	3.5
threonine^{68} O_γ–O	3.2	3.2		
valine^{68} $C_{\gamma2}$–O			3.3, 2.8	3.2
threonine^{68} O_γ–C	3.5	3.6		
valine^{68} $C_{\gamma2}$–C			3.1	3.5
histidine^{64} N_ϵ–threonine^{68} O_γ	3.2	3.6		
histidine^{64} N_ϵ–valine^{68} $C_{\gamma2}$			3.8	3.4
threonine^{68} O_γ–histidine^{64} O	2.7	2.6		
valine^{68} $C_{\gamma2}$–histidine^{64} O			3.4	3.2

[a] Data from Kuriyan et al. (1986). Two orientations of the CO ligand were modeled in this work, with occupancies of 78% and 22%. The first of the values quoted is for the conformation with the higher occupancy. [b] Data from Quillin et al. (1993) for recombinant sperm whale MbCO purified from *Escherichia coli*. [c] θ = 180° corresponds to a linear Fe–C–O angle. The Fe–C and C–O distances were restrained during refinement to 1.8 and 1.2 Å, respectively. The Fe–O distance was restrained to 3.0 Å, thus effectively restraining the Fe–C–O angle to 180°. [d] This angle is defined according to Kuriyan et al. (1986). It is the angle between the O–C–Fe plane and the C–Fe–NC plane; φ = 0° corresponds to the CO eclipsing the Fe–NC bond and φ = 90° to CO bond eclipsing the Fe–ND bond. [e] The plane is defined by a least-squares fit to the four pyrrole nitrogen atoms of the heme group. A negative value indicates a displacement toward the ligand.

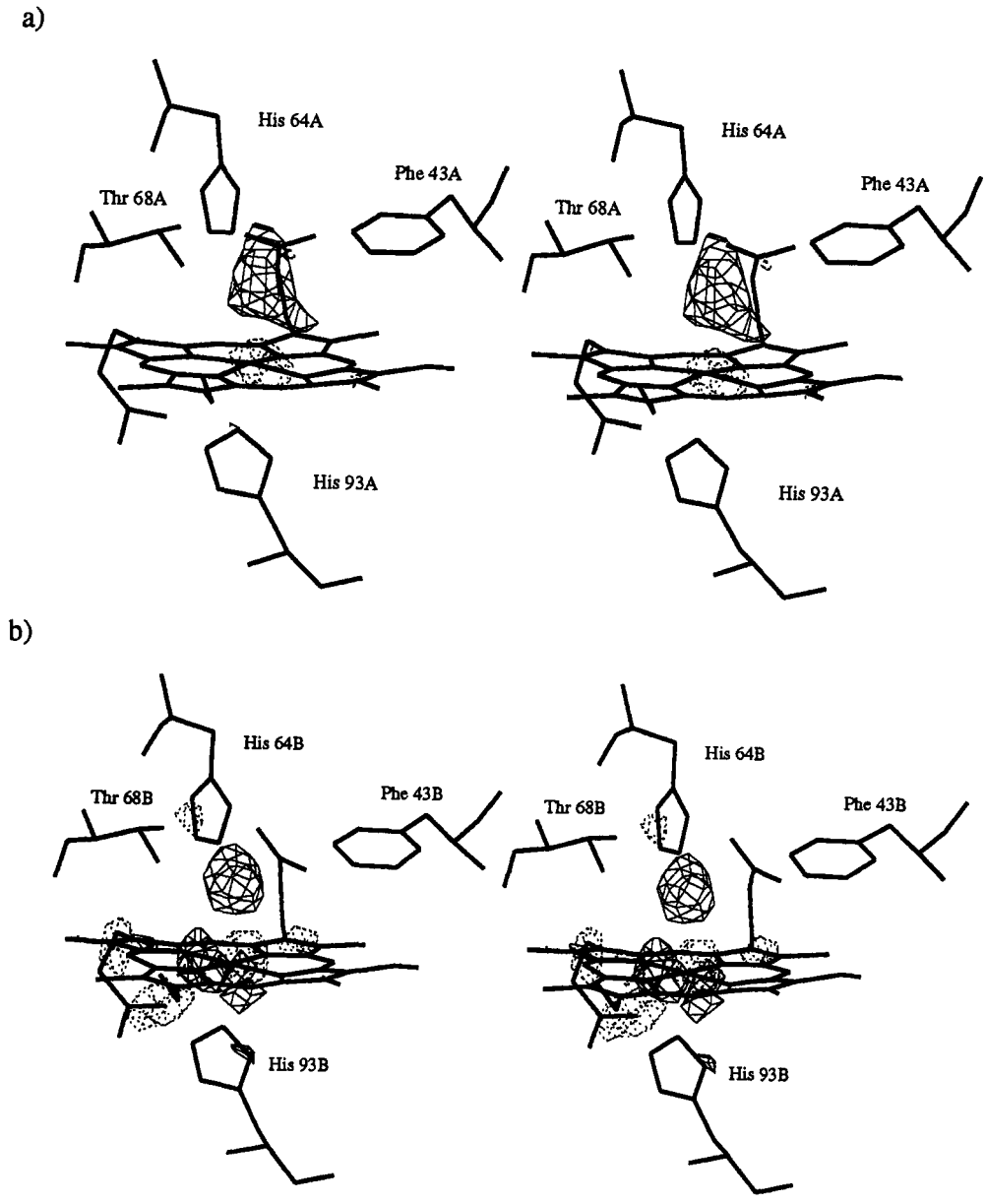

FIGURE 3: Stereo view of initial threonine[68] deoxyMb electron density maps calculated with coefficients $F_{obsDeoxy\text{-}Thr68} - F_{calcCO\text{-}Thr68}$ and $\alpha_{calcCO\text{-}Thr68}$ contoured at 3σ (full lines) and -3σ (dotted lines. The electron density is superimposed on the MbCO model (thick lines) from which the ligand has been removed. The phases were calculated with the CO and all water molecules removed from the refined structure of threonine[68] MbCO. (a) The heme environment in the A molecule. (b) The corresponding region in the B molecule.

that this dipole moment destabilizes bound CO (Smerdon et al., 1991).

Details of the CO geometry in the final structure are set out in Table IV. In both molecules of the asymmetric unit, the Fe–C–O angle has refined from approximately 180° in the initial model to 162° in the final structure against the geometrical restraints. This angle falls in the range, 160°–170°, of Fe–C–O angles reported by Quillin et al. (1993) for wild-type and three distal histidine mutants of sperm whale myoglobin crystallized in space group *P*6 (glutamine[64], leucine[64], and glycine[64]). It is lower than that refined in normal adult hemoglobin (175°) or hemoglobin Cowtown (169°) but considerably larger than those for the two conformations modeled in the 1.5-Å resolution structure of sperm whale MbCO in space group $P2_1$ (140° and 120°) (Derewenda et al., 1990; Kuriyan et al., 1986). As for other carbonmonoxymyoglobin structures (Kuriyan et al., 1986; Quillin et al., 1993), there has been a rotation of the side chain of histidine[64] about its C_α–C_β bond, moving the imidazole ring away from the bound CO. There is no evidence for rotation of the residue-64 side chain about the C_β–C_γ bond, which would allow the N_ϵ-H group to make a hydrogen-bonding interaction with the hydroxyl of threonine[68].

Threonine deoxyMb Structure. The crystals of threonine[68] deoxyMb were more closely isomorphous with the crystals of threonine[68] MbCO than with the crystals of the met forms of wild-type or threonine[68] myoglobin, as judged from the mean isomorphous differences of 14%, 26%, and 37%, respectively. Initially, a difference Fourier map was calculated using coefficients $F_{obsDeoxy\text{-}Thr68} - F_{calcCO\text{-}Thr68}$ and $\alpha_{calcCO\text{-}Thr68}$. The map, which was calculated with the CO omitted from the model, is displayed in the vicinity of the heme pockets in Figure 3. There is evidence from these maps that the structures of the two heme pockets are not identical; in the B molecule the density is consistent with the presence of an uncoordinated water molecule adjacent to the N_ϵ atom of histidine[64], while in the A molecule the shape and size of the electron density peak in this region imply a more complicated structure.

The final threonine[68] deoxymyoglobin structure, which includes 2482 non-hydrogen atoms and 109 water molecules, has an R_{cryst} of 19.8% for all data (18 200 reflections) between 7- and 2.1-Å resolution and reasonable geometry (Table III).

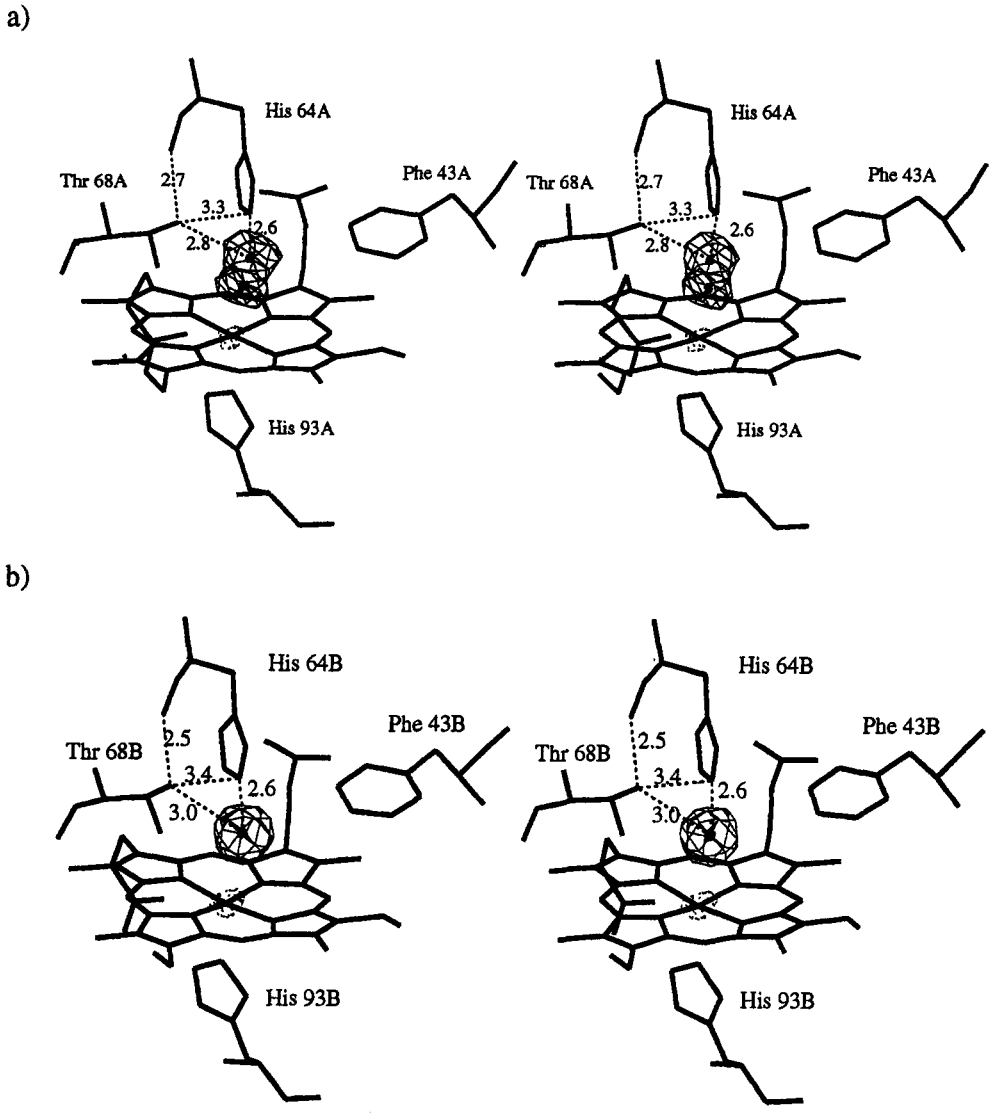

FIGURE 4: Stereo diagrams showing the environment of the heme in the A (a) and B (b) molecules of the refined threonine[68] deoxyMb structure. Electron density from the corresponding $F_o - F_c$ map, contoured at $+3\sigma$ (full lines) and -3σ (dotted lines), calculated with the distal pocket waters omitted from the phasing, is shown. For both molecules of the asymmetric unit, the peak value of the electron density shown in the figure is 1.6 times the highest noise peak in the map. The interatomic distances are shown in angstroms. The hydroxyl group of threonine[68] can donate a hydrogen bond to the main-chain >C=O of histidine[64] while accepting a hydrogen bond from the noncoordinated (or coordinated) water molecule.

F_o-F_c maps for the final structure calculated with the distal pocket waters removed from the phasing are shown in Figure 4. As was suggested by the initial maps, the water structure in the distal pocket is inconsistent between the two molecules of the asymmetric unit. For the B molecule, the distal pocket electron density peaks in F_o-F_c and $2F_o$-F_c maps can be assigned unambiguously to a water molecule residing 3.0 Å from the iron and within hydrogen-bonding distance of the hydroxyl group of threonine[68] and the N_ϵ-H of histidine[64]. For the A molecule, we have interpreted the maps as representing two partially occupied water sites, the first noncovalently bound in the distal pocket and the second coordinated to the iron. The occupancies of these water molecules have been assigned on the basis of the relative size of the corresponding electron density peaks as 0.7 and 0.3 for the noncoordinated and coordinated species, respectively.

Some of the details of the interactions made by these distal pocket waters are presented in Table V. Regardless of the relative sizes of the two water peaks in the A molecule, it is clear from Figure 4 and Table V that the noncoordinated distal pocket water molecule in threonine[68] deoxymyoglobin is able to form two strong hydrogen bonds, with the N_ϵ-H of histidine[64] acting as a proton donor and the Oγ of threonine[68] acting as a proton acceptor. In wild-type sperm whale deoxymyoglobin, a single hydrogen-bonding interaction with the N_ϵ-H of histidine[64] is made by the distal pocket water molecule, and it is expected that this interaction will also occur in wild-type pig deoxymyoglobin (Phillips, 1981; Quillin et al., 1993). The additional hydrogen-bonding interaction provided by threonine[68] stabilizes the water molecule in the mutant relative to the wild-type protein. As for the MbCO structure, there is no evidence of any direct interaction between the N_ϵ-H group of histidine[64] and the Oγ of threonine[68].

The reasons that underlie the discrepancies in the maps between the A and the B molecules of the asymmetric unit cannot be identified with certainty. The most likely possibility is that a small proportion of the A molecules had autooxidized. Based on the relative occupancies of the distal pocket water molecules, this would represent a net oxidation of less than 20% of the total iron atoms in the crystal. The presence of some oxidized protein is consistent with a UV/vis spectrum of the dissolved crystals recorded 24 h after data collection.

Infrared Spectrum of the CO Complex. The infrared spectrum of CO bound to threonine[68] pig myoglobin is shown

Table V: Comparison of Interatomic Distances in the Heme Pocket of Pig Threonine^{68} deoxyMb with the Corresponding Interatomic Distances in Sperm Whale Deoxymyoglobin

distance (Å)	threonine^{68} deoxyMb A molecule	threonine^{68} deoxyMb B molecule	sperm whale[a] deoxyMb
Fe–histidine^{93} N_ϵ	2.1	2.2	2.1
Fe–H_2O	1.9, 3.5[b]	3.0	3.8, 4.2
Fe–plane of pyrrole nitrogens[c]	0.08	0.18	0.30, 0.32
H_2O–histidine^{64} N_ϵ	2.7, 2.7[b]	2.6	3.1, 2.7
H_2O–threonine^{68} O_γ	3.5, 2.8[b]	3.0	
H_2O–valine^{68} $C_{\gamma 2}$			3.5, 3.5
histidine^{64} N_ϵ–threonine^{68} O_γ	3.3	3.4	
histidine^{64} N_ϵ–valine^{68} $C_{\gamma 2}$			3.3, 3.3
threonine^{68} O_γ–histidine^{64} O	2.7	2.5	
valine^{68} $C_{\gamma 2}$–histidine^{64} O			3.4, 3.3

[a] The first value given is for the $P2_1$ crystal form of native sperm whale deoxymyoglobin (Phillips, 1981); the second value is from the data for the *P6* crystal form of recombinant wild-type sperm whale myoglobin (Quillin et al., 1993). [b] The first value given corresponds to the coordinated water molecule and the second to the noncoordinated water (see text for explanation). [c] This plane is defined by a least-squares fit to the four pyrrole nitrogen atoms. The positive values indicate displacement toward the proximal histidine.

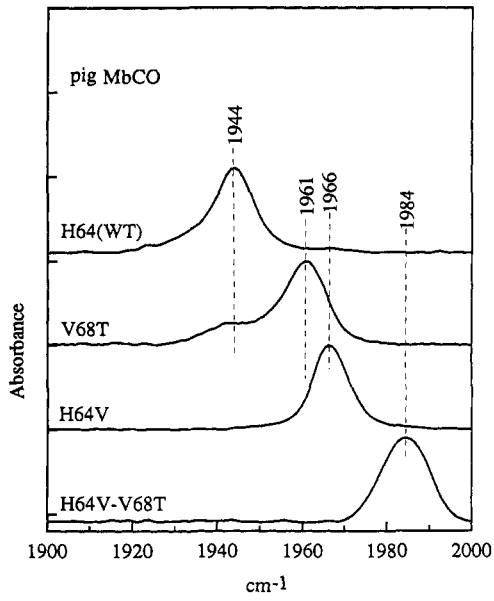

FIGURE 5: IR spectra in the region 1900–2000 cm^{-1} for wild-type (H64(WT), top curve), threonine^{68} (V68T), valine^{64} (H64V), and valine^{64}–threonine^{68} (H64V-V68T, bottom curve) pig carbonmonoxymyoglobins in 0.1 M phosphate, 1 mM EDTA, pH 7.0, at room temperature.

in Figure 5 and compared to spectra for wild-type pig myoglobin, the valine^{64} single mutant, and the valine^{64}–threonine^{68} double mutant. A summary of the observed CO stretching frequencies (ν_{CO}) and ligand-binding parameters for these proteins is presented in Table VI. The results for the threonine^{68} mutant are quite surprising in view of the X-ray structures presented here, the ligand-binding constants, and most previous interpretations of CO stretching frequencies. In previous work with position-64 mutants of sperm whale myoglobin, there was a correlation between increases in K_{CO} and increases in ν_{CO} which was initially attributed to relief of steric hindrance [e.g., Morikis et al. (1989)]. This behavior is also shown by the valine^{64} and valine^{64}–threonine^{68} pig mutants, which have 3–10-fold higher affinities for CO than the wild-type protein and exhibit single CO stretching bands at 1966 and 1984 cm^{-1}, respectively (Figure 5, Table VI). However, even though the affinity of pig myoglobin for CO (K_{CO}) decreases ~5-fold and the Fe–C–O angle remains ~160°, there is a marked shift of absorbance intensity from the wild-type band at 1944 cm^{-1} (ν_1) to 1961 cm^{-1} (ν_0) when valine^{68} is replaced by threonine.

DISCUSSION

Polarity and Ligand Association Rate Constants. The loss of polarity in the heme pocket following replacement of the distal histidine in sperm whale myoglobin by aliphatic side chains leads to accelerated rates of ligand binding (Springer et al., 1989; Carver et al., 1990). X-ray crystallographic and spectroscopic studies of these mutants and similar recombinant hemoglobins suggest an inverse correlation between the ligand-binding rates and the stability of the noncoordinated water molecule in the deoxy form of these proteins (Mathews et al., 1989; Rohlfs et al., 1990; Quillin et al., 1993). This trend is emphasized by the opposing effects of increasing the polarity of the distal pocket in the threonine^{68} mutant. The crystal structure of threonine^{68} deoxymyoglobin demonstrates that the distal pocket stereochemistry is essentially unaffected by the mutation. As a result, the decreased rates of ligand binding (Table VI) can be attributed unambiguously to stabilization of the noncoordinated water molecule by the threonine hydroxyl. Since this noncoordinated water molecule must be displaced before the iron atom becomes accessible to the ligand, the hydrogen-bonding interactions with histidine^{64} and threonine^{68} markedly inhibit ligand binding. A detailed discussion of the effects of distal pocket mutations on the individual picosecond and nanosecond kinetic events for O_2, CO, and NO binding has been presented (Carver et al., 1990; Smerdon et al., 1991).

Contributions of Steric Hindrance and Polarity to Ligand Affinity. Direct steric hindrance by the distal histidine^{64} has traditionally been used to explain why the affinity of myoglobin for CO is lowered. This idea is supported by the high-resolution crystal structure of sperm whale myoglobin in space group $P2_1$, which shows a markedly bent Fe–C–O geometry and displacement of the histidine^{64} side chain away from the bound ligand (Kuriyan et al., 1986). Initial ligand-binding experiments with position-64 mutants of sperm whale myoglobin supported this interpretation. When histidine^{64} is replaced by glycine, valine, leucine, and phenylalanine, CO affinity increases 3–30-fold (Rohlfs et al., 1990). However, Quillin et al. (1993) have recently shown that the Fe–C–O angle in the P6 crystal form is 165 ± 10° for the wild-type and the glycine^{64}, glutamine^{64}, and leucine^{64} sperm whale myoglobin mutants. The results in Tables IV and VI support the view that CO affinity cannot be predicted from the coordination geometry of bound CO. The valine^{68}-to-threonine substitution causes a 5-fold decrease in affinity but no change in either the ligand geometry or the positions of the protein residues in the distal pocket. The lack of correlation between bound ligand geometry and affinity implies that direct steric hindrance plays a lesser role and polarity plays a greater role in regulating CO affinity than previously thought. However, Ray et al. (1993) have pointed out that the force constants for Fe–C–O distortion are so large that steric hindrance may inhibit CO binding without causing large changes in the conformation of the bound ligand.

The results in Table VI are most readily interpreted if the displacement of distal pocket water is the major equilibrium barrier to ligand binding. When histidine^{64} is replaced by an aliphatic residue, there are no polar groups near the iron, and as a result there is no distal pocket water in deoxymyoglobin to inhibit ligand binding (Quillin et al., 1993). This accounts for the higher association rate constant and the higher CO affinity of the valine^{64} pig myoglobin mutant. The lower

Table VI: Rate Constants for O_2 and CO Binding and the Infrared Stretching Frequencies for the CO Complexes of Wild-Type, Threonine[68] (V68T), Valine[64] (H64V), and Valine[64]–Threonine[68] (H64V-V68T) Pig Myoglobin at pH 7.0, 0.1 M Phosphate, 20 °C[a]

protein	k'_{O_2} (μM^{-1} s^{-1})	k_{O_2} (s^{-1})	K_{O_2} (μM^{-1})	k'_{CO} (μM^{-1} s^{-1})	k_{CO} (s^{-1})	K_{CO} (μM^{-1})	ν_0 (%) (cm^{-1})	ν_1 (%) (cm^{-1})	ν_3 (%) (cm^{-1})
wild-type	17	14	1.2	0.78	0.020	39	1968(5)	1944(83)	1930(12)
V68T	2.8	39	0.072	0.61	0.079	7.6	1961(80)	1944(20)	(<1)
H64V	110	10 000	0.011	6.4	0.050	130	1966(100)	(0)	(0)
H64V-V68T	100	4000	0.025	27	0.063	430	1984(100)	(0)	(0)

[a] The kinetic parameters for wild-type and threonine[68] myoglobin were taken from Smerdon et al. (1991). Those for the other mutants were measured for this work. The percentages of the CO conformers were estimated from the intensity ratios by peak heights. The frequency subscripts ν_0, ν_1, and ν_3 correspond to the A_0, A_1, and A_3 conformer designations presented by Caughey, Frauenfelder, Champion, and others (Braunstein et al., 1988; Morikis et al., 1989) and refer to components with CO stretching frequencies in the regions ~1965, ~1945, and ~1930 cm^{-1}, respectively.

oxygen affinity and higher dissociation rate result from the lack of a hydrogen bond donor to stabilize bound O_2. In contrast, the threonine[68] substitution stabilizes distal pocket water, which decreases markedly the affinity of pig myoglobin for both ligands. All of these effects can be expressed without any change in the geometry of the bound ligand or the distal pocket since they involve noncoordinated water and are electrostatic in origin.

CO Affinity and Stretching Frequency. The data in Figure 5 and Table VI demonstrate that there is a dramatic and unexpected lack of correlation between CO affinity and the stretching frequency of the bound ligand. Both the histidine[64]-to-valine mutation and the valine[68]-to-threonine mutation cause an increase in ν_{CO} from 1944 to 1966 and 1961 cm^{-1}, respectively, but in the former case K_{CO} is increased 3-fold and in the latter case K_{CO} is decreased 5-fold. This result, coupled with the lack of changes in the Fe–C–O geometry among the various position-64 mutants and the threonine[68] mutant, suggests that the CO stretching frequency is governed more by electrostatic considerations than by direct steric hindrance with either residue-64 or -68. Lin et al. (1990) reached a similar conclusion based on resonance Raman studies of a series of E7 and E11 mutants of hemoglobin.

Li and Spiro (1988) and others have shown that there is a reciprocal relationship between ν_{CO} and ν_{FeC}, implying that when the bond order of Fe–C decreases, that for C–O increases. This inverse relationship also applies to the mutants listed in Table VI. Biram et al. (1991) have reported that the dominant ν_{FeC} values for wild-type, threonine[68], valine[64], and the valine[64]–threonine[68] pig myoglobins are 508, 496, 491, and 479 cm^{-1}, respectively, implying that both mutations weaken the Fe–C bond, either singly or in combination, whereas ν_{CO} increases. This observation correlates roughly with the increase in the CO dissociation rate constants observed for these mutants but not with the overall affinities (Table VI). The latter discrepancy can be resolved by taking into account the free energy required to displace distal pocket water molecules before CO binds, which is very small in the case of the valine[64] mutants but very large for the threonine[68] myoglobin single mutant, which also contains a distal histidine.

Li and Spiro's interpretation of CO stretching frequencies suggests that proton donors will increase the degree of back-bonding by the iron atom, which in turn increases the order of the Fe–C bond and decreases the order of the C–O bond. This explains why wild-type pig myoglobin has a lower CO stretching frequency (major peak at ~1945 cm^{-1}) compared to that observed for the valine[64] mutant (1966 cm^{-1}), in which the hydrogen bond donor at residue-64 has been removed. The threonine[68] substitution produces the same effect by placing the negative portion of the β-hydroxyl dipole adjacent to the bound ligand. The presence of this negative electrostatic field inhibits back-bonding by the iron, decreases the Fe–C bond order, and increases the order of the C–O bond. This results in a 16–18-cm^{-1} increase in ν_{CO} regardless of whether histidine or valine is present at position-64 (*viz.* spectra for threonine[68] and valine[64]–threonine[68] mutants in Figure 5).

A key element of Li and Spiro's (1988) explanation is that histidine[64] can form a hydrogen bond, albeit a weak one, with bound CO. The observation of Schoenborn and co-workers that the proton of the imidazole side chain of histidine[64] is on the N_δ atom in MbCO and not on N_ϵ as in MbO_2 appears to rule out hydrogen bonding to bound CO (Hanson & Schoenborn, 1981; Cheng & Schoenborn, 1991; Phillips & Schoenborn, 1981). However, it is possible that a small fraction of the tautomer with a proton at N_ϵ is present which stabilizes bound CO and perturbs its IR spectrum but that the fraction is too small to be detected crystallographically. Recently, Kitigawa, Hochstrasser, and co-workers (Lian et al., 1993) have suggested that the degree of hydration of MbCO markedly affects tautomerization of the distal histidine. Based on the work of Brown et al. (1983), it appears that increasing hydration favors protonation of the N_ϵ and deprotonation of N_δ. It should also be noted that the neutron diffraction studies were carried out on the $P2_1$ crystal form of sperm whale myoglobin, which contains much less water than the more loosely packed P6 crystal form and shows a markedly bent Fe–C–O geometry (Phillips et al., 1990; Quillin et al., 1993).

Further support for polarity being the key determinant of the CO stretching frequency comes from the resonance Raman work of Ray et al. (1993) on sterically constrained Fe(II) porphyrins. These workers observed large variations in the C–O and Fe–C stretching frequencies of the CO adducts of two capped model heme compounds whose crystal structures show very similar Fe–C–O geometries. They concluded that polar interactions with either amide or ester/ether groups in the linker arms of the "cap", rather than geometric distortions, are the primary determinants of the ligand vibrational frequencies. Boxer and co-workers have replaced valine[68] with asparagine in human myoglobin and recorded the IR absorption spectrum of this mutant (Balasubramanian et al., 1993a,b). This mutation causes a marked decrease in ν_{CO} from ~1945 to ~1915 cm^{-1} at room temperature, and we have observed the same phenomenon for the corresponding mutant in sperm whale myoglobin. The simplest interpretation is that an additional hydrogen bond is formed between bound CO and protons on the N_δ atom of the asparagine side chain at the E11 position. In the Li and Spiro model, this would promote further back-bonding by the Fe atom, increase the order of the Fe–C bond, and decrease that for the C–O bond even further. These effects are the opposite of those observed for the threonine[68] mutant, where the negative dipole of the β-OH inhibits back-bonding and increases ν_{CO} to ~1960 cm^{-1}. Verification of this interpretation will require determination of the crystal structure of the asparagine[68] mutant.

Autooxidation. Perhaps the most dramatic effect of the valine[68]-to-threonine mutation is the 50-fold increased rate of autooxidation (Brantley et al., 1993). In native myoglobin, autooxidation occurs by both a bimolecular reaction between

molecular oxygen and deoxymyoglobin with a weakly bound water molecule and a unimolecular mechanism involving the dissociation of the neutral superoxide radical from the oxygenated complex (Brantley et al., 1993). In the case of the threonine[68] mutant, the negative portion of the hydroxyl dipole facilitates protonation of bound O_2 and the subsequent dissociation of HO_2, causing the unimolecular mechanism to predominate at all oxygen concentrations (Brantley et al., 1993).

Conclusion. Regardless of the exact interpretation, the results presented here show that there is no correlation between K_{CO}, ν_{CO}, and the observed Fe–C–O geometry in wild-type and mutant myoglobins. These results suggest strongly that the displacement of distal pocket water molecules is a major determinant of overall ligand affinity and that electrostatic fields near the binding site regulate Fe–ligand bond strengths as measured by dissociation rate constants or IR stretching frequencies.

ACKNOWLEDGMENT

We would like to thank Guy and Eleanor Dodson for encouragement and critical discussion.

REFERENCES

Balasubramanian, S., Lambright, D. G., & Boxer, S. G. (1993a) *Proc. Natl. Acad. Sci. U.S.A. 90*, 4718–4722.

Balasubramanian, S., Lambright, D. G., Marden, M. C., & Boxer, S. G. (1993b) *Biochemistry 32*, 2202–2212.

Biram, D., Garratt, C. J., & Hester, R. E. (1991) in *Spectroscopy of Biological Molecules*, 433–434 (Hester, R. E., & Girling, R. B., Eds.), Royal Society of Chemistry, Cambridge, U.K.

Brammer, R., Helliwell, J. R., Lamb, W., Liljas, A., Moore, P. R., Thompson, A. W., & Rathbone, K. (1988) *Nucl. Instrum. Methods A271*, 678–687.

Brantley, R. E., Smerdon, S. J., Wilkinson, A. J., Singleton, E. W., & Olson, J. S. (1993) *J. Biol. Chem. 268*, 6995–7010.

Braunstein, D., Ansari, A., Berendzen, J., Cowen, B. R., Egeberg, K. D., Fraunfelder, H., Hong, M. K., Ormos, P., Sauke, T. B., Scholl, R., Schulte, A., Sligar, S. G., Springer, B. A., Steinbach, P. J., & Young, R. D. (1988) *Proc. Natl. Acad. Sci. U.S.A. 85*, 8497–8501.

Brown, W. E., Sutcliffe, J. W., & Pulsinelli, P. D. (1983) *Biochemistry 22*, 2914–2922.

Carver, T. E., Rohlfs, R. J., Olson, J. S., Gibson, Q. H., Blackmore, R. S., Springer, B. A., & Sligar, S. G. (1990) *J. Biol. Chem. 265*, 20007–20020.

Carver, T. E., Olson, J. S., Smerdon, S. J., Krzywda, S., Wilkinson, A. J., Gibson, Q. H., Blackmore, R. S., Ropp, J. D., & Sligar, S. G. (1991) *Biochemistry 30*, 4697–4705.

Carver, T. E., Brantley, R. E., Singleton, E. W., Arduini, R. M., Quillin, M. L., Phillips, G. N., & Olson, J. S. (1992) *J. Biol. Chem. 267*, 14443–14450.

CCP4 (1986) in *A Suite of Programs for Protein Crystallography*, SERC Daresbury Laboratory, Warrington, U.K.

Cheng, X., & Schoenborn, B. P. (1991) *J. Mol. Biol. 220*, 381–399.

Derewenda, Z., Dodson, G., Emsley, P., Harris, D., Nagai, K., Perutz, M., & Renaud, J.-P. (1990) *J. Mol. Biol. 211*, 515–519.

Dickerson, R. E., & Geis, I. (1983) in *Haemoglobin: Structure, Function, Evolution and Pathology*, Benjamin/Cummings, Menlo Park, CA.

Egeberg, K. D., Springer, B. A., Sligar, S. G., Carver, T. E., Rohlfs, R. J., & Olson, J. S. (1990) *J. Biol. Chem. 265*, 11788–11795.

Hadju, J., Machin, P. A., Campbell, J. W., Greenhough, T. J., Clifton, I. J., Zurek, S., Gover, S., & Johnson, L. N. (1987) *Nature 329*, 178–181.

Hanson, J. C., & Schoenborn, B. P. (1981) *J. Mol. Biol. 153*, 117–146.

Helliwell, J. R., Habash, J., Cruickshank, D. W. J., Harding, M. M., Greenhough, T. J., Campbell, J. W., Clifton, I. J., Elder, M., Machin, P. A., Papiz, M. Z., & Zurek, S. (1989) *J. Appl. Crystallogr. 22*, 483–497.

Hendrickson, W., & Konnert, J. H. (1980) in *Biomolecular Structure Function Conformation and Evolution* (Srinivisan, R., Ed.) Vol. 1, pp 43–57, Pergamon, Oxford, U.K.

Jones, T. A. (1982) in *Computational Crystallography* (Sayre, D., Ed.) pp 303–317, Clarendon Press, Oxford, U.K.

Kuriyan, J., Wilz, S., Karplus, M., & Petsko, G. (1986) *J. Mol. Biol. 192*, 133–154.

Li, X.-Y., & Spiro, T. G. (1988) *J. Am. Chem. Soc. 110*, 6024–6033.

Lian, T., Locke, B., Kitigawa, T., Nagai, M., & Hochstrasser, R. M. (1993) *Biochemistry 32*, 5809–5819.

Lin, S.-H., Yu, N.-T., Tame, J., Shih, D., Renaud, J.-P., Pagnier, J., & Nagai, K. (1990) *Biochemistry 29*, 5562–5566.

Lindahl, M., Liljas, A., Habash, J., Harrop, S., & Helliwell, J. R. (1992) *Acta Crystallogr. B48*, 281–285.

Luzzati, V. (1952) *Acta Crystallogr. A5*, 802–820.

Mathews, A. J., Rohlfs, R. J., Olson, J. S., Tame, J., Renaud, J.-P., & Nagai, K. (1989) *J. Biol. Chem. 264*, 16573–16583.

Mims, M. P., Porras, A. G., Olson, J. S., Noble, R. W., & Peterson, J. A. (1983) *J. Biol. Chem. 258*, 14219–14232.

Morikis, D., Champion, P. M., Springer, B. A., & Sligar, S. G. (1989) *Biochemistry 28*, 4791–4800.

Oldfield, T. J., Smerdon, S. J., Dauter, Z., Petratos, K., Wilson, K. S., & Wilkinson, A. J. (1992) *Biochemistry 31*, 8732–8739.

Peng, S.-M., & Ibers, J. A. (1976) *J. Am. Chem. Soc. 98*, 8032–8036.

Phillips, S. E. V. (1980) *J. Mol. Biol. 142*, 531–554.

Phillips, S. E. V. (1981) in *The X-ray Structure of Deoxy-Mb (pH 8.5) at 1.4 Å Resolution*, Brookhaven Protein Data Bank, Brookhaven National Laboratory, Upton, NY.

Phillips, S. E. V., & Schoenborn, B. P. (1981) *Nature 292*, 81–82.

Phillips, G. N., Arduini, R. M., Springer, B. A., & Sligar, S. G. (1990) *Proteins 7*, 358–365.

Quillin, M. L., Arduini, R. M., Olson, J. S., & Phillips, G. N. (1993) *J. Mol. Biol.* (in press).

Ray, G. B., Li, X.-Y., Ibers, J. A., Sessler, J. L., & Spiro, T. G. (1993) *J. Am. Chem. Soc.* (submitted).

Rohlfs, R. J., Mathews, A. J., Carver, T. E., Olson, J. S., Springer, B. A., Egeberg, K. D., & Sligar, S. G. (1990) *J. Biol. Chem. 265*, 3168–3176.

Scheidig, A. J., Pai, E. F., Schlichting, I., Corrie, J., Reid, G. P., Wittinghofer, A., & Goody, R. S. (1991) *Philos. Trans. R. Soc. London A340*, 263–272.

Schlichting, I., Almo, S. C., Rapp, G., Wilson, K. S., Petratos, K., Lentfer, A., Wiitinghofer, A., Kabsch, W., Pai, E. F., Petsko, G. A., & Goody, R. S. (1990) *Nature 345*, 309–315.

Singer, P. T., Smalas, A., Carty, R. P., Mangel, W. F., & Sweet, R. M. (1993) *Science 259*, 669–673.

Smerdon, S. J., Dodson, G. G., Wilkinson, A. J., Gibson, Q. H., Blackmore, R. S., Carver, T. E., & Olson, J. S. (1991) *Biochemistry 30*, 6252–6260.

Springer, B. A., Egeberg, K. D., Sligar, S. G., Rohlfs, R. J., Mathews, A. J., & Olson, J. S. (1989) *J. Biol. Chem. 264*, 3057–3060.

Takano, T. (1977) *J. Mol. Biol. 110*, 569–584.